

# A nonstationary search parameter for internal multiple prediction

Kris Innanen

## ABSTRACT

With the internal multiple prediction algorithm re-formulated in terms of the output time, the opportunity arises for the search limiting parameter to be varied according to some schedule  $\epsilon(t)$ . Any prior knowledge suggesting that within a single trace *this* output time requires aggressive prediction, but *that* output time requires cautious prediction, can be used to guide an appropriate selection of  $\epsilon(t)$ . Here we will consider two fairly obvious types of criterion for selection: data driven selection strategies and strategies driven by geological prior knowledge. 1D and zero offset synthetic and physical modelling lab data are used to find situations where the precision of predictions is increased beyond what would be available given any single fixed  $\epsilon$  parameter. The promising results are suggestive that a much broader study of selection strategies for  $\epsilon$  as functions of time, frequency, offset, lateral wavenumber, source and receiver horizontal slownesses, etc., is warranted.

## INTRODUCTION

CREWES is engaged in a set of projects designed to comprehensively address the problem of internal multiples on land. The projects are based on inverse scattering series internal multiple attenuation technology (Araújo, 1994; Weglein et al., 1997, 2003), with domain modifications (Sun and Innanen, 2015) and supporting technology (e.g., adaptive subtraction; see Keating et al., 2015) tuned to issues associated with land application. The purpose of this paper is to examine the practical importance of a re-casting of the standard form algorithm into the time domain, in particular its importance relative to the precision with which a multiple can be estimated amongst events in a “crowded” trace or gather.

In a companion paper (Innanen, 2015), the formula for 1D time domain internal multiple prediction,

$$\text{IM}_t(t) = \int_{-\infty}^{\infty} dt' s(t' - t) \int_{\alpha(t,t')}^{\beta(t)} dt'' s(t' - t'') s(t''), \quad (1)$$

where  $s(t)$  is an input trace, and where, fixing the search limiting parameters  $\epsilon_1 = \epsilon_2 = \epsilon$ ,

$$\begin{aligned} \alpha(t, t') &= t' - (t - \epsilon) \\ \beta(t) &= t - \epsilon, \end{aligned} \quad (2)$$

was derived. Apart from directing its output to a different domain, equation (1) is mathematically equivalent to the standard frequency domain 1D internal multiple prediction formula. Thus any differences between its output and that of standard formulae must be attributable to practical calculation details. Of these details, one in particular, concerning the choice of  $\epsilon$ , has the capacity to increase the precision with which internal multiples are distinguished from nearby primaries. This may have particular application in land interbed multiple prediction, where “close interference between primaries and internal multiples occurs” (Luo et al., 2011).

## Prediction domains and options for $\epsilon$ nonstationarity

The parameter  $\epsilon$ , first introduced in the work of Coates and Weglein (1996), is selected in order to impose a lower limit on the separation of data variations satisfying the *lower-higher-lower* criterion for combining primary and multiple subevents (Weglein et al., 1997, 2003). Incorrectly small values produce artifacts which interfere with primaries; incorrectly large values leave thin bed multiples unpredicted. Most implementations select  $\epsilon$  once for a given data set based on its dominant frequency, producing an output whose response to  $\epsilon$  is stationary. Indeed, in order for the prediction to operate properly,  $\epsilon$  must remain a constant as the integrals are carried out. However, within this constraint it is possible to create output whose response to the parameter is nonstationary, by making  $\epsilon$  a function of the output variables. For instance Innanen and Pan (2015) demonstrated how a 1.5D prediction in standard form, e.g.,

$$\text{IM}_{k\omega}(k_g, \omega) = \int_{-\infty}^{\infty} dt e^{i\omega t} S(k_g, t) \int_{-\infty}^{t-\epsilon} dt' e^{-i\omega t'} S(k_g, t') \int_{t'+\epsilon}^{\infty} dt'' e^{i\omega t''} S(k_g, t''), \quad (3)$$

can be cleaned of large angle artifacts by making  $\epsilon \propto k_g$ . In fact, any assertion that  $\epsilon$  for the output pair  $(k_g, \omega)|_0$  should be different from that at pair  $(k_g, \omega)|_1$  can be tested with equation (3) and an appropriate choice of  $\epsilon = \epsilon(k_g, \omega)$ . Testable assertions about  $\epsilon$  are restricted to those concerning the output variables of the formula. In this sense, the choice of domain in which the formula is applied has nontrivial consequences. In the companion paper (Innanen, 2015) formulas for  $\text{IM}_{k\omega}$ ,  $\text{IM}_{kt}$ ,  $\text{IM}_{xt}$  and the core formula  $\text{IM}_t$  were discussed: these provide arenas for testing nonstationarity in  $\epsilon$  of the forms  $\epsilon(k_g, \omega)$ ,  $\epsilon(k_g, t)$ , and  $\epsilon(x_g, t)$  and  $\epsilon(t)$  respectively. All deserve consideration, but in this paper we focus on the possibilities associated with  $\epsilon(t)$ , which seem to hold the most promise for real problems in multiple prediction.

### JUSTIFICATION FOR TIME-NONSTATIONARITY IN $\epsilon$

The internal multiple prediction algorithm works by combining three sub-events which are separated from one another in vertical travel-time or pseudo-depth in the seismic record. For instance, a triplet of primaries combines to predict a first order internal multiple. Let  $d$  represent the average separation distance between a given triplet of sub-events. On land, internal multiples are a mixture of those generated within small scale heterogeneities and thin bedding, often in the near surface (Luo et al., 2011), and those generated by distinct and more widely spaced formations. The former, appearing at relatively early times for shallow generators, are predicted by sub-event triplets for which  $d$  is relatively small. The latter, growing more dominant at later times in the same circumstances, are predicted by combining sub-event triplets for which  $d$  is relatively large. Near surface thin bedding, in other words, causes  $d$  to become a nonstationary characteristic of the seismic record. Because  $d$  is a primary factor in selecting  $\epsilon$ , nonstationarity in  $d$  implies nonstationarity in  $\epsilon$ . The idea illustrated in Figure 1, where differences in sub-event raypath lengths at earlier and later times are found.

To demonstrate the idea of nonstationarity in  $\epsilon$  numerically, consider the 1D numerical example in Figures 2–5. Figure 2 is the velocity model, designed with a shallow, high velocity bed overlying a deeper structure of interest. The 1D reflectivity method of Gan-

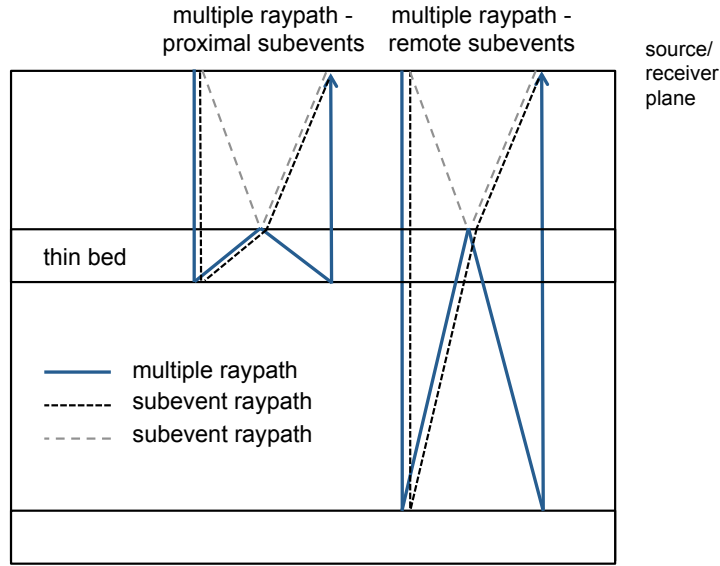


FIG. 1. A near-surface region of thin bedding imposes a pattern on the output of the multiple prediction operator. Multiples at earlier times in the output prediction are predicted by combining sub-events that are proximal to one another in time (on the left, the sub-event ray paths, drawn with black and grey dashed lines, have similar lengths). Multiples at later times are predicted with sub-events that are distant from one another (on the right, the black and grey dashed sub-event ray paths have very different lengths).

ley (1981), as implemented by Margrave (2015) was employed to simulate a 1D normal incidence seismic response with an 80Hz causal wavelet, a 1ms sample interval, and a coincident source and receiver at  $z = 0$ . The trace is plotted in Figure 3, with arrows indicating the dominant multiples. A feature of the Ganley method is that multiples can be turned on and off, and so in later plots we will be able to compare predictions against a trace containing the exact multiples.

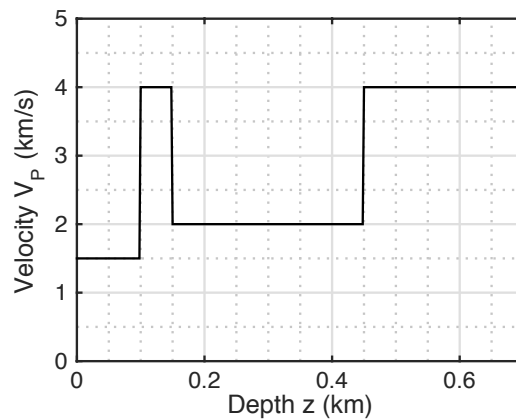


FIG. 2. Velocity model with shallow thin bedding.

We first use this trace as input to the 1D internal multiple prediction algorithm in equation (1), selecting a relatively large constant  $\epsilon$  value of 30 sample points, roughly three times the wavelet period  $1/f_{dom}$ . The results are plotted in Figure 4. In Figure 4a the input

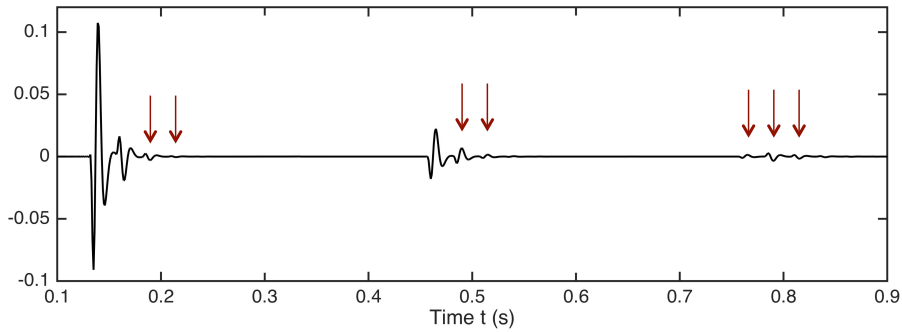


FIG. 3. Trace generated over the model in Figure 2. Multiple reflections are labelled with arrows. Two closely spaced primaries are visible between 0.1-0.2s, and the third primary is visible as the leading event in the cluster near 0.5s.

trace is plotted as a black solid line, with the prediction overlain in red (and upshifted to be more easily seen). Also overlain is a dashed black line representing the relative  $\epsilon$  value, which in this case was 30. In Figure 4b the prediction, again in red, is compared against the exact multiples.

The nonstationarity of the response to  $\epsilon$  is visible in Figure 4b. The deepest multiples plotted, arriving between 0.7-0.9s, are all well captured by the prediction. Moving to earlier times, the cluster of multiples arriving at around 0.5s is partially predicted, but with the dominant leading multiple largely missed. At still earlier times, the multiples near 0.2s are minimally predicted. The large value of  $\epsilon$ , while satisfactory for the later multiples, is too restrictive to properly predict the earlier primaries.

In light of this, we attempt a prediction with a smaller and more aggressive constant value of  $\epsilon$ , this time 10 sample points, which is very close to the wavelet period. The results are plotted in Figure 5, which is organized in the same way as Figure 4. (Because the dashed line in Figure 5a is the relative  $\epsilon$  value, and we have again used a fixed value, it appears identical to the previous case.) Examining Figure 5b, we see that the change has not affected the prediction of the later time multiples, but the smaller  $\epsilon$  value has led to a more or less complete prediction of the multiple energy in the cluster near 0.5s. The earliest multiples have also been predicted very completely, but here a new issue is visible. The low  $\epsilon$  value has admitted artifacts aligning with the second primary, which would experience significant alterations if we were to attempt an adaptive subtraction.

Clearly the appropriate response to this is to dial back the aggressiveness of  $\epsilon$ . But, because  $\epsilon = 10$  was just small enough to correctly predict the multiples at 0.5s, this cannot be done completely without reducing the efficacy of the later time predictions. No fixed  $\epsilon$  value will completely suffice.

However, with access to an algorithm in which the prediction occurs output time point by output time point, we have the freedom to select a nonstationary  $\epsilon = \epsilon(t)$ . Leaving the matter of how to select an optimal  $\epsilon(t)$  schedule unresolved for the moment, let us see that a nonstationary  $\epsilon$ , varying between 10 and 30 sample points, creates the desired prediction. Figure 6 contains the results. In Figure 6a, the nonstationary  $\epsilon(t)$ , selected to smoothly step

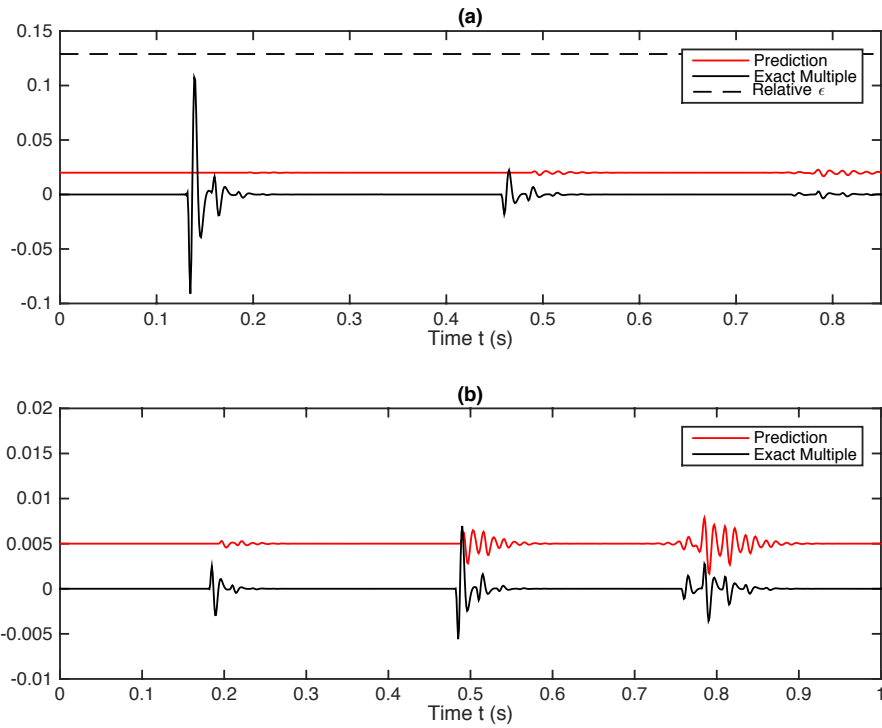


FIG. 4. Effect of large, fixed  $\epsilon$ . (a) Input trace (black) vs. prediction (red); (b) prediction (red) vs. exact multiple (black).

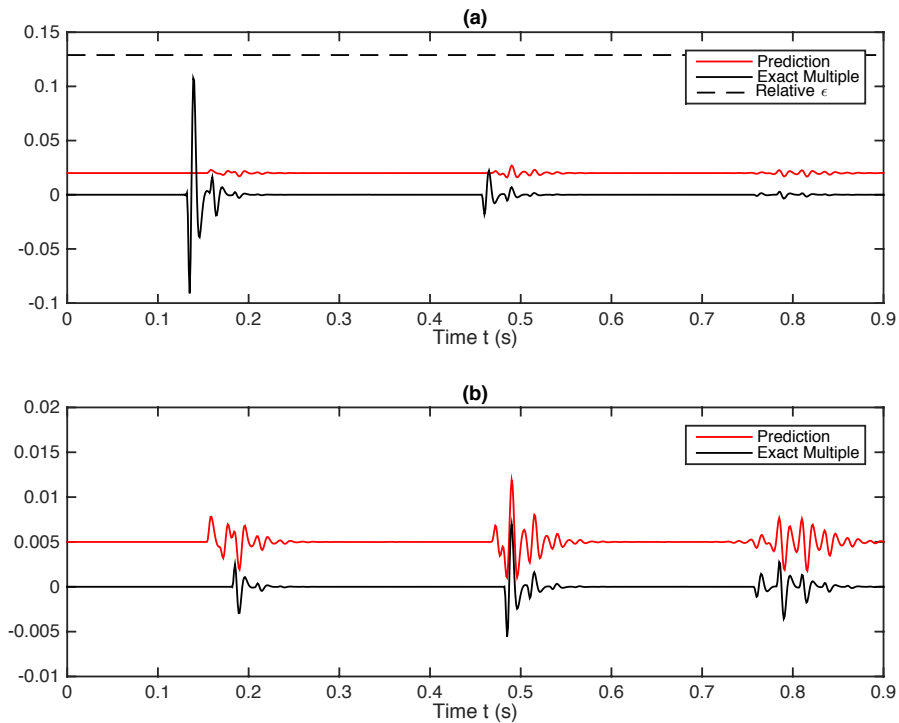


FIG. 5. Effect of small, fixed  $\epsilon$ . (a) Input trace (black) vs. prediction (red); (b) prediction (red) vs. exact multiple (black).

up and down between 10 and 30 sample points, is plotted. In Figure 6b the salutary effect on the prediction is visible.

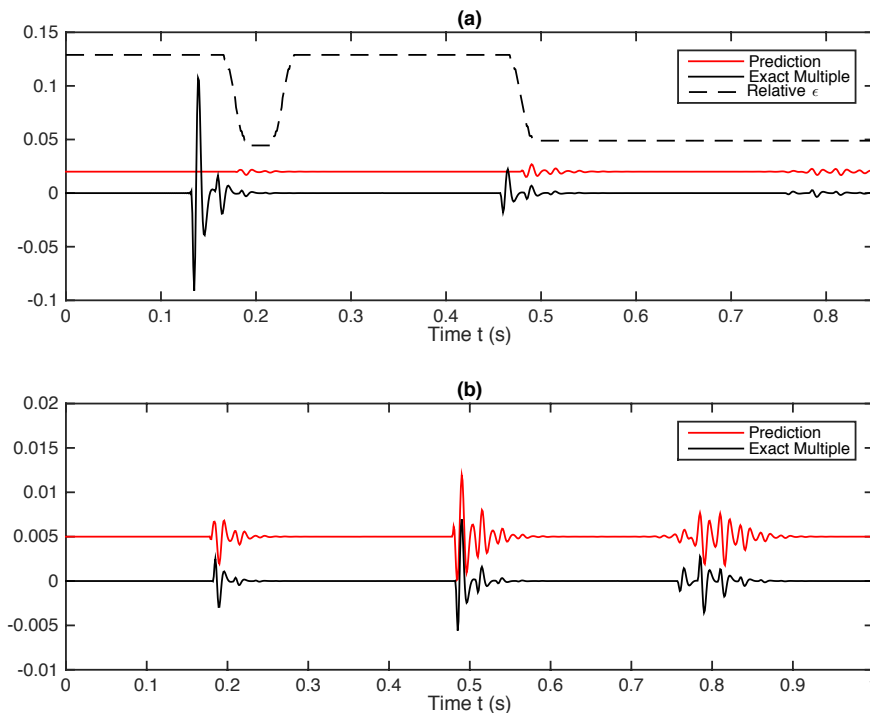


FIG. 6. Effect of variable  $\epsilon(t)$ . (a) Input trace (black) vs. prediction (red), with scaled  $\epsilon(t)$ , varying between 10 and 30 sample points, plotted as a dashed black line; (b) prediction (red) vs. exact multiple (black).

We conclude then that a judiciously selected  $\epsilon(t)$ , stepping up and down the aggressiveness with which sub-events are combined, gives rise to multiple estimates whose precision is not attainable with any stationary  $\epsilon$  choice.

## EXAMPLES

In the previous section we demonstrated that if we know with reasonable certainty where multiple rich output times are on a seismic trace or gather, a nonstationary  $\epsilon(t)$  can be set up to enhance the precision of the prediction. We next turn to possible approaches to formulating the  $\epsilon(t)$ . The purpose of these examples is not to be dogmatic, but to propose some straightforward strategies for optimizing the prediction parameter.

### Data driven $\epsilon(t)$ estimation

In Figure 6 a backdrop value of relatively large  $\epsilon$ , on the order of  $3/f_{dom}$ , which corresponds to “cautious” prediction, was perturbed to a lower, more “aggressive” value in regions known to contain mostly multiple energy. Having some prior knowledge of such regions is not out of the question, but coming up with a generally applicable procedure for determining these areas if they are unknown is not really possible. It may be more feasible to go the other way: to set up a more aggressive background  $\epsilon$  value, and perturb it upward

in regions where caution is necessary. This could be applied in a general way by adopting a general principle about multiple energy vs primary energy. For instance, we could tie the upward perturbation of  $\epsilon(t)$  to the general ambient energy level of the trace: thus, in areas rich in primaries, where the energy in the trace is high,  $\epsilon(t)$  would jump to a higher, more cautious value.

In the next two figures we illustrate a prototype version of such an  $\epsilon(t)$  model. We use the same synthetic data as in the previous case. In Figure 7 we first attempt the prediction with the fixed background  $\epsilon$  set at an aggressive 10 sample points, corresponding to roughly  $1/f_{dom}$ . The result is the same as that in Figure 5. In Figure 7b the blue exact multiple is precisely overlain on the red prediction. The focus here is on the leading edges of the multiple clusters – at 0.2s and 0.5s the red prediction has significant energy well before the actual multiples.

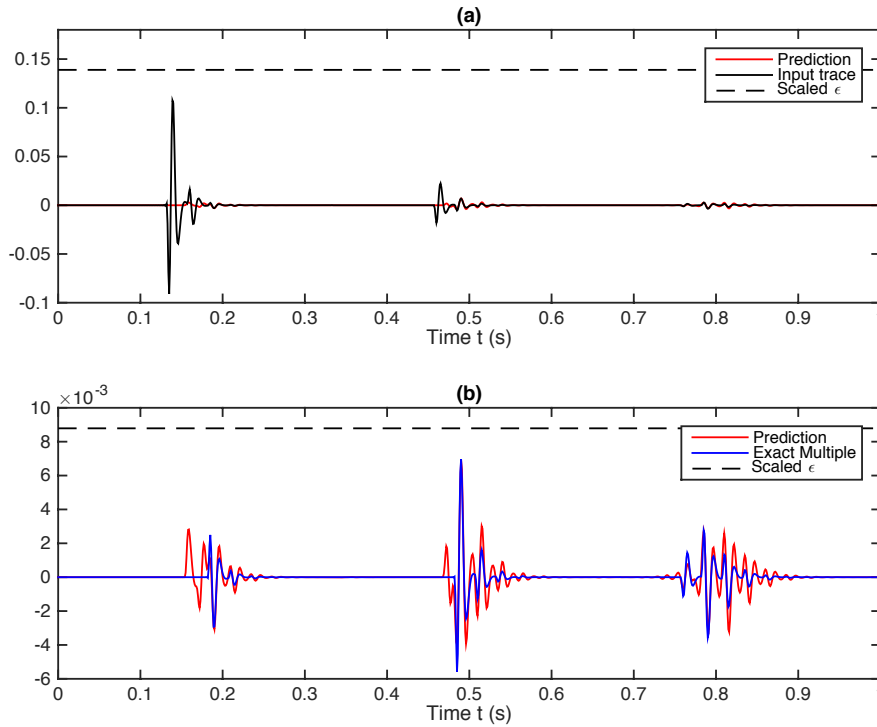


FIG. 7. Prediction with fixed  $\epsilon$  of 10 sample points. (a) Input trace (black) vs prediction (red), with  $\epsilon(t)$  plotted as a dashed line. (b) Prediction (red) vs. exact multiple (blue).

We next apply an upward perturbation to the fixed  $\epsilon$  value. A smoothed Hilbert envelope of the data is calculated and added to  $\epsilon$  after being normalized such that its maximum value is the cautious endmember  $3/f_{dom}$ . This produces a nonstationary  $\epsilon(t)$  which grows from an aggressive base value up towards a maximum height, altering the value such that it is more cautious in regions where the trace energy is high. Provided high energy in the trace corresponds to regions rich in primaries, this represents a more or less general procedure for varying  $\epsilon(t)$ . The  $\epsilon(t)$  is plotted over the trace and the prediction in Figure 8a, and again over top of the prediction vs exact multiple comparison in Figure 8b. Comparing Figure 8b with the results with those of Figure 6b, we see roughly the same level of increased

precision is possible with a data driven  $\epsilon(t)$  estimation.

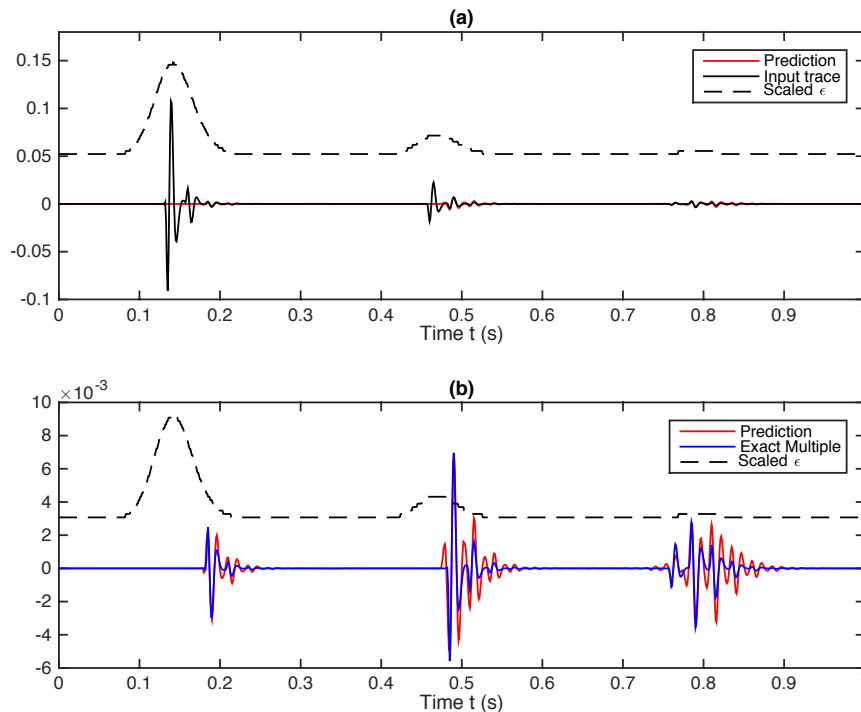


FIG. 8. The consequences to prediction of a data driven time-variant  $\epsilon(t)$ . (a) Input trace (black) vs prediction (red). Primary subevents near 0.2s and 0.5s are very close together. (b) Prediction (red) using an  $\epsilon(t)$  determined from the Hilbert envelope of the trace (dashed black line), compared against the exact multiple (blue).

### Geological prior knowledge: physical modelling data example

Another possible approach to the practical selection of  $\epsilon(t)$  is to be guided by the partial information content of a blocked well log. With some sense of regions of the data where multiples might dominate over primaries, the  $\epsilon(t)$  function can be selected to decrease in those regions and grow elsewhere. To exemplify this, we consider a physical modelling laboratory data set consisting of a zero offset section acquired over a roughly layered medium constructed with large impedance contrasts (Hernandez and Innanen, 2014).

The zero offset section is plotted in Figure 9. Traces can be extracted from this section and to within a reasonable degree of accuracy be treated with 1D methods. The data are divided into two subregions, the middle region being the first, and the left- and right-hand edges being the second. The former are traces whose source/receiver pair were over top of an aluminum slab; the latter are traces acquired beyond the lateral extent of the slab.

A profile view of the lab model is illustrated in Figure 10a, and the associated  $V_P$  profile is sketched alongside it (Figure 10b). In this study we will use this latter profile as a proxy for a blocked well log, and use the information such a blocked log contains to act as a guide for the choice of the search parameter time dependence.

A representative trace (CMP number 200) is extracted from the central region of the

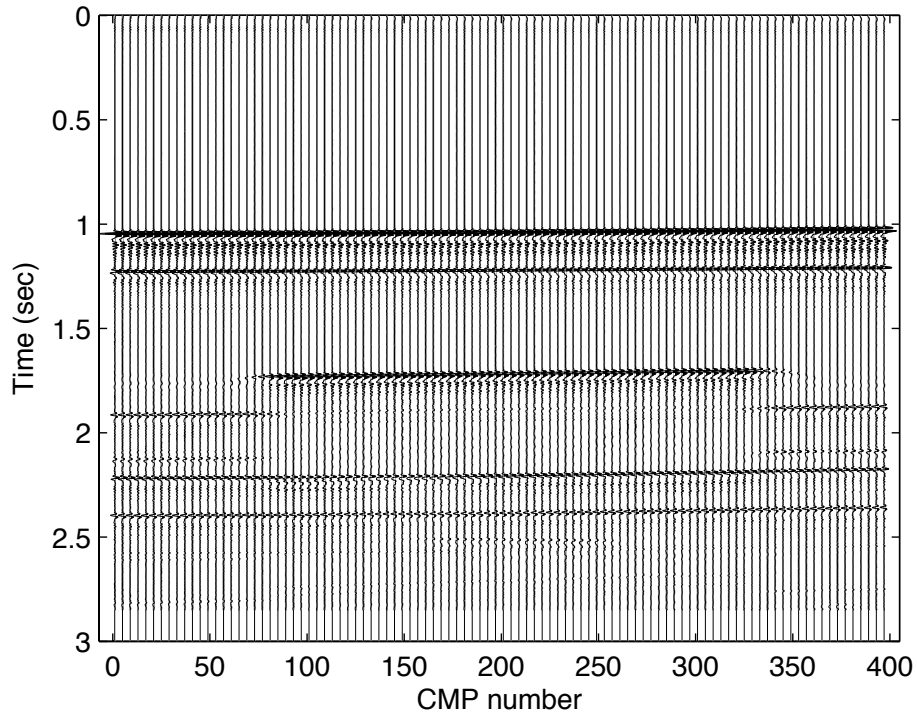


FIG. 9. Zero offset physical modelling laboratory section. The central regions correspond to source/receiver pairs overlying an aluminum slab; left and right hand edges correspond to regions beyond the extent of the slab. See Figure 10.

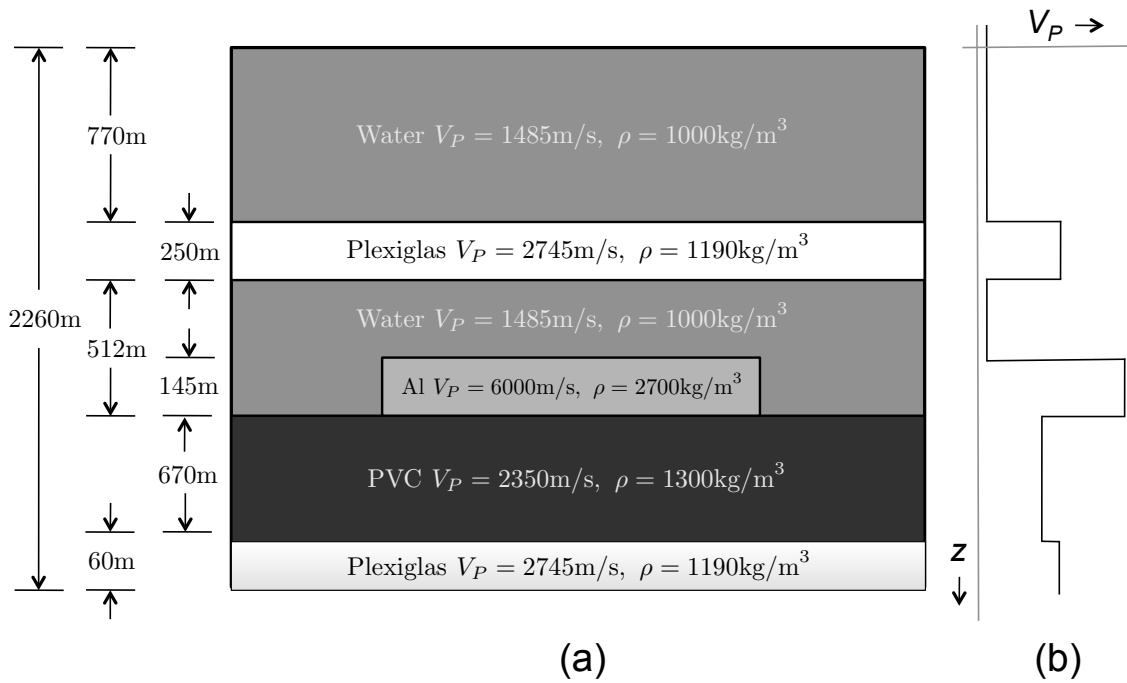


FIG. 10. Profile view of the physical model, adapted from Hernandez and Innanen (2014). (a) 2D side view; (b) vertical  $V_P$  profile through the central part of the model. The velocity profile has the bearing of blocked well log with the blocking carried out at very large scale.

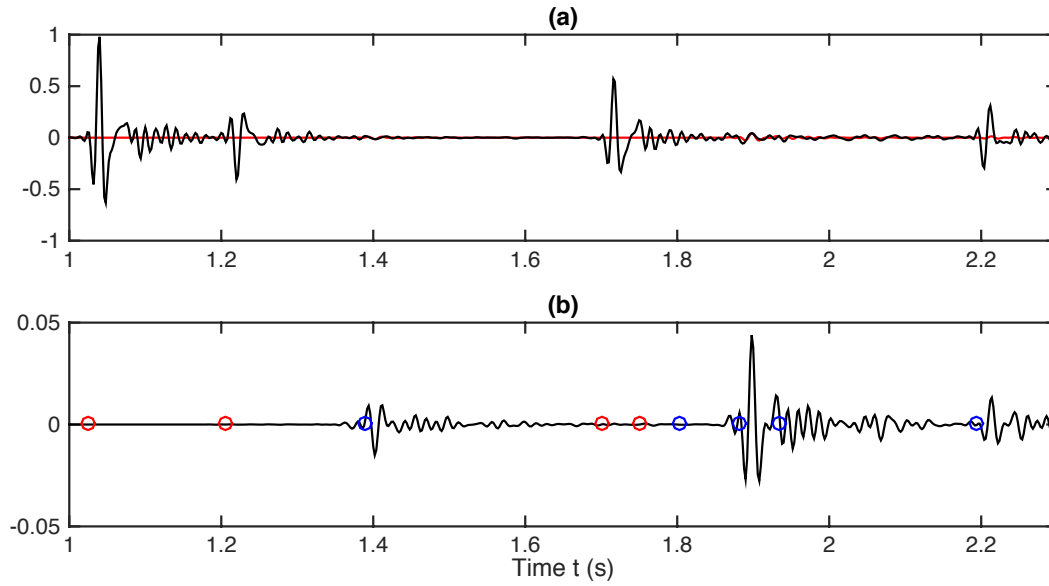


FIG. 11. (a) Input trace (black) with prediction (red). (b) Prediction (black) with expected arrival times of primaries indicated with red dots, and expected arrival times of multiples indicated with blue dots.

section, and is subject to the time-domain internal multiple prediction operation. At first we select a large, constant  $\epsilon$  value, corresponding to 70 sample points or 140ms, which is roughly  $7/f_{dom}$ . The results are plotted in Figure 11. In Figure 11a, the input trace (black) is plotted alongside the prediction (red), and in Figure 11b a zoom-in on the prediction (black) is plotted. The red dots are the expected arrival times of the first four major primaries as calculated using the proxy for the blocked logs in Figure 10b. These match well with the large arrivals in Figure 11a. The blue dots are the expected arrival times of some of the major internal multiples, also calculated from the information in Figure 10b.

Having chosen a large, and cautious value for  $\epsilon$ , the danger is that multiples in the trace which must be predicted by nearby subevents may be missed. An example of this is visible in Figure 11b: the multiple expected near 1.8s does not appear in the prediction (that is, a blue dot appears with no accompanying variation in the prediction). The reason this particular multiple is missing is that it corresponds to a reverberation between the top and bottom of the aluminum slab. The primaries that combine to predict this multiple therefore also come from the top and bottom of the slab, and so, because the  $V_P$  of the aluminum is very high, the two primaries are very near one another, well within the separation minimum imposed by  $\epsilon = 7/f_{dom}$ , and thus are missed in the cautious prediction.

In order to predict such a multiple, we must evidently lower  $\epsilon$ . Running the prediction with progressively lower values, we eventually arrive at the result illustrated in Figure 12, which is calculated with a fixed  $\epsilon$  value of 35 sample points, or 70ms, or roughly  $3/f_{dom}$ , i.e.,  $3\times$  the dominant period of the trace. The plots are organized in the same way. This time, the multiple at 1.8s (Figure 12b) is predicted, which means the new minimum separation distance is sufficiently small that the primaries from the top and bottom of the aluminum are accommodated. However, with this smaller  $\epsilon$  the danger has now be-

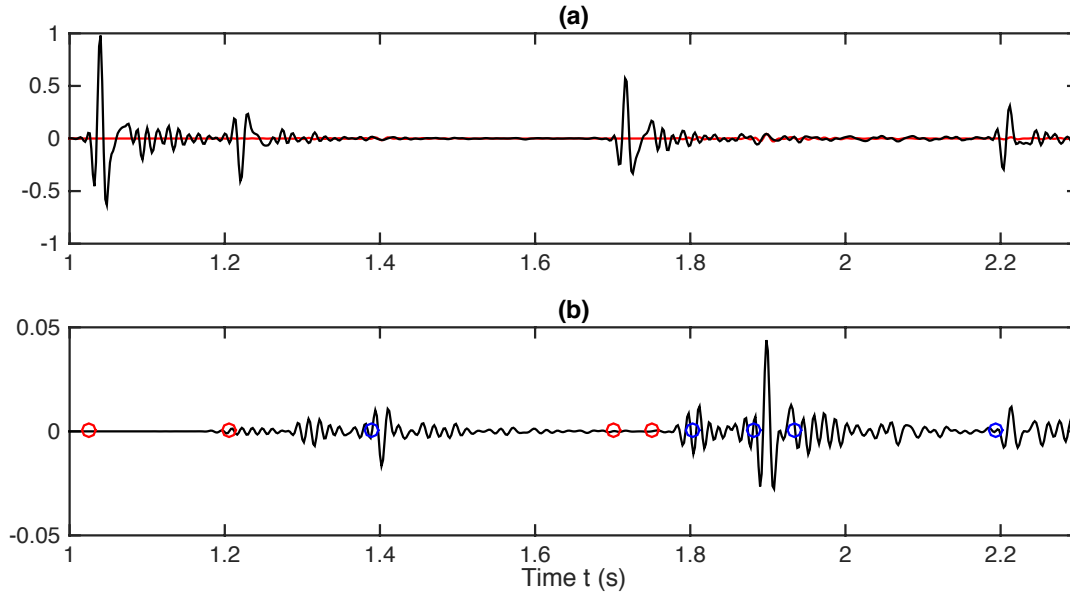


FIG. 12. (a) Input trace (black) with prediction (red). (b) Prediction (black) with expected arrival times of primaries indicated with red dots, and expected arrival times of multiples indicated with blue dots.

come instead that artifacts correlated with primaries will appear. And, this is the case: the prediction near the primary time at 1.2s sees the onset of energy which was not present previously. So, again in this case we see that the  $\epsilon$  value needed near 1.8s is different from the one which should be in play near 1.2s, justifying the use of nonstationary  $\epsilon(t)$ .

The need for a nonstationary  $\epsilon(t)$  has been established using information which might plausibly be available to a processor: the red and blue dots in Figures 11 and 12 are derived from the coarse-grained information in Figure 10, which, again, is a proxy for a well log blocked to include the most important horizons. This same geologically-derived prior information, in the form of isolated points where multiples and primaries are likely to congregate, also forms a rough criterion whereby the schedule  $\epsilon(t)$  can be selected.

The prediction result involving an  $\epsilon(t)$  variation jumping between 70-100 and 35 sample points, is illustrated in Figure 13. The discontinuous jumps in  $\epsilon(t)$ , which are plotted proportionally as a dashed line in Figure 13b, are selected such that aggressive prediction is favoured in regions dominated by expected multiples (blue dots), and cautious prediction is favoured in other regions. Focusing on the times 1.2s and 1.8s, a balance has been struck in which the significant multiples are predicted without introducing glaring artifact energy near the primaries.

## CONCLUSIONS

Every time a form of the inverse scattering series internal multiple prediction algorithm is re-formulated in terms of new output variables, the opportunity arises for the search limiting parameter  $\epsilon$  to vary as a function of these new variables. In this paper we have focused on the opportunities afforded by time domain prediction, inasmuch as it makes possible the

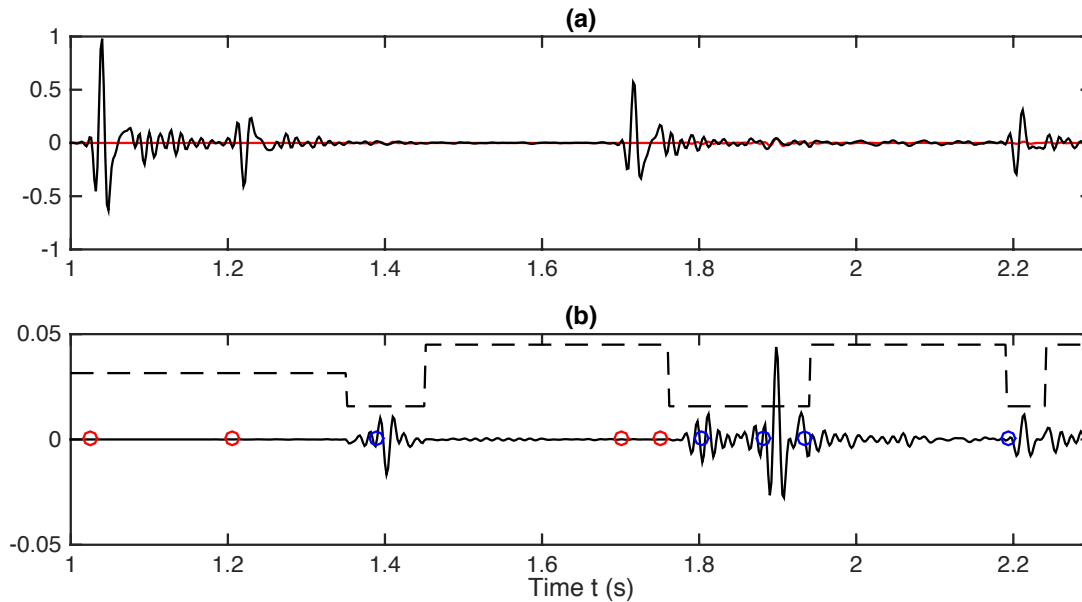


FIG. 13. (a) Input trace (black) with prediction (red). (b) Prediction (black) with expected arrival times of primaries indicated with red dots, and expected arrival times of multiples indicated with blue dots. The dashed line is the nonstationary  $\epsilon(t)$  function, plotted proportionally. The real  $\epsilon$  numbers vary between a maximum of 100 sample points and 35 sample points.

introduction of a search limiting schedule  $\epsilon(t)$ . Any prior knowledge which tells the processor that *this* output time requires (or can afford) aggressive prediction, but *that* output time requires (or can afford) cautious prediction, can be used to guide an appropriate selection of  $\epsilon(t)$ . Data driven selection strategies and strategies driven by geological prior knowledge are obvious possibilities, and with synthetic and physical modelling lab data it is possible to easily find situations where the precision of predictions is increased beyond what would be available given any single fixed  $\epsilon$  parameter. We view this as the tip of the iceberg, with study of selection strategies for  $\epsilon$  as functions of time, frequency, offset, lateral wavenumber, source and receiver horizontal slownesses, etc., being warranted.

## ACKNOWLEDGEMENTS

We thank the sponsors of CREWES for continued support. This work was funded by CREWES industrial sponsors and NSERC (Natural Science and Engineering Research Council of Canada) through the grant CRDPJ 461179-13.

## REFERENCES

- Araújo, F. V., 1994, Linear and non-linear methods derived from scattering theory: backscattered tomography and internal multiple attenuation: Ph.D. thesis, Universidade Federal da Bahia.
- Coates, R. T., and Weglein, A. B., 1996, Internal multiple attenuation using inverse scattering: results from prestack 1 & 2d acoustic and elastic synthetics: SEG Technical Program Expanded Abstracts, 1522–1525.
- Ganley, D. C., 1981, A method for calculating synthetic seismograms which includes the effects of absorption and dispersion: *Geophysics*, **46**, No. 8, 1100–1107.

- Hernandez, M. J., and Innanen, K. A., 2014, Identifying internal multiples using 1d prediction: physical modelling and land data examples: *Canadian Journal of Geophysical Exploration*, **39**, No. 1, 37–47.
- Innanen, K. A., 2015, Time-domain internal multiple prediction: CREWES Annual Report, **27**.
- Innanen, K. A., and Pan, P., 2015, Large dip artifacts in 1.5D internal multiple prediction and their mitigation: CSEG Expanded Abstracts.
- Keating, S., Sun, J., Pan, P., and Innanen, K. A., 2015, Nonstationary  $l_1$  adaptive subtraction with application to internal multiple attenuation: CREWES Annual Report, **27**.
- Luo, Y., Kelamis, P. G., Fu, Q., Huo, S., Sindi, G., Hsu, S., and Weglein, A. B., 2011, Elimination of land internal multiples based on the inverse scattering series: *The Leading Edge*, **30**, No. 8, 884–889.
- Margrave, G. F., 2015, Stratigraphic filter and Q estimation: CSEG Expanded Abstracts.
- Sun, J., and Innanen, K. A., 2015, 1.5D internal multiple prediction in the plane wave domain: CSEG Expanded Abstracts.
- Weglein, A. B., Araújo, F. V., Carvalho, P. M., Stolt, R. H., Matson, K. H., Coates, R. T., Corrigan, D., Foster, D. J., Shaw, S. A., and Zhang, H., 2003, Inverse scattering series and seismic exploration: *Inverse Problems*, , No. 19, R27–R83.
- Weglein, A. B., Gasparotto, F. A., Carvalho, P. M., and Stolt, R. H., 1997, An inverse-scattering series method for attenuating multiples in seismic reflection data: *Geophysics*, **62**, No. 6, 1975–1989.